IOP Publishing | Royal Swedish Academy of Sciences Physica Scripta

Phys. Scr. **T171** (2020) 014047 (9pp) https://doi.org/10.1088/1402-4896/ab4e52

Damaging of inclined/misaligned castellated tungsten surfces exposed to a large number of repetitive QSPA plasma loads

V A Makhlai[1,2,4], S S Herashchenko[1], N N Aksenov[1], O V Byrka[1], I E Garkusha[1,2], M Wirtz[3] and B Spilker[3]

[1] National Science Center 'Kharkov Institute of Physics and Technology', Institute of Plasma Physics, Kharkiv, Ukraine
[2] V.N. Karazin Kharkiv National University, Kharkiv, Ukraine
[3] Forschungszentrum Jülich GmbH, Institut für Energie- und Klimaforschung, D-52425, Jülich, Germany

E-mail: makhlay@ipp.kharkov.ua

Received 19 June 2019, revised 30 September 2019
Accepted for publication 16 October 2019
Published 6 March 2020

Abstract

In fusion devices like ITER and DEMO, transient events could result in substantial damage in the form of erosion of exposed surfaces due to the extreme energy loads. Castellated tungsten mock-ups were chosen as reference design for the plasma-facing components (PFC) of fusion devices. The material response of these mock-ups is crucial for the lifetime of the PFC and needs to be evaluated for a large number of repetitive plasma impacts. Therefore, an experimental investigation of erosion processes on castellated tungsten surfaces has been performed within the powerful quasi-stationary plasma accelerator QSPA Kh-50 with conditions that simulated a failure of the edge localized mode control in ITER. The surface energy load measured with a calorimeter was 0.9 MJ m^{-2}, i.e. above the melting (0.6 MJ m^{-2}) and below the evaporation (1.1 MJ m^{-2}) thresholds of tungsten. The plasma pulse duration was 0.25 ms. Intense overheating of the castellated edge, which interacted with the plasma first, was observed alongside the formation of an excrescence of shifted material during the first few tens of plasma pulses. The maximum number of ejected particles was registered after the plasma pulses, i.e. during the cooling process. Nevertheless, the amount of particles ejected during the plasma exposure increased with the plasma pulse number. The splashing of droplets and ejection of dust was suppressed on flat surfaces of castellated monoblocks, whereas the edges were identified as the main source of ejected particles.

Keywords: tungsten, transient heat loads, QSPA plasma accelerator, plasma-surface interaction, ITER ELM, castellated surfaces

(Some figures may appear in colour only in the online journal)

1. Introduction

In fusion devices like ITER (Latin for 'the way') and DEMO (DEMOnstration Power Plant), transient events could result in significant damage in the form of erosion of exposed material surfaces due to the incident extreme energy loads [1, 2]. Tungsten (W) is currently the main candidate as plasma facing material for the highly loaded divertor components of future fusion devices. W has demonstrated a high erosion resistance under exposure to plasma particles and neutrals. Moreover, W has the highest melting threshold of any metal and demonstrated a low activation level under neutron irradiation. The castellated geometry of tungsten Plasma-Facing Components (PFC) is considered as reference design for the divertor surface in fusion devices [2]. One of the primary problems of a full metal divertor is the appearance and motion

[4] Author to whom any correspondence should be addressed.

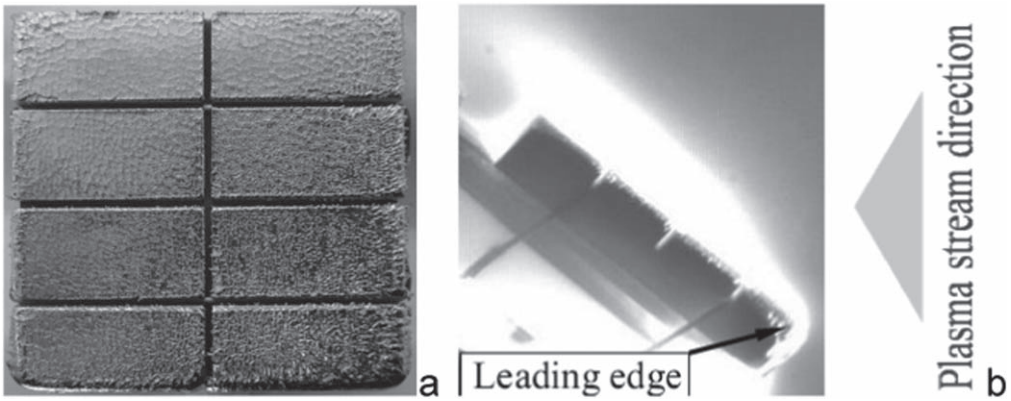

Figure 1. General view of the castellated target ($5 \times 5 \times 1\,\mathrm{cm}^3$) exposed to 200 plasma pulses (a). Image of the plasma-surface interaction (PSI) with the inclined target (b), recorded at the beginning of the PSI ($t_{\mathrm{exposure}} = 1.2$ ms, i.e. frame corresponding to 0–1.2 ms after the start of the PSI).

of melted material on the monoblock surfaces during plasma disruptions or/and the development of Edge Localized Modes (ELMs) in H-mode operation. The melt layer is subjected to external forces such as surface tension, gradients of both plasma pressure and recoil pressure of evaporating material, and Lorentz force ($j \times B$) among others. Melt motion driven by external forces produces significant macroscopic erosion of materials [2]. This process is considered as the most important one from the point of view of the lifetime of metallic armors and the emission of molten/solid dust particles [3–10].

Repetitive melting of tungsten by power transients originating from ELMs has been studied in ASDEX Upgrade [11–14]. Tungsten samples were exposed to H-mode discharges at the outer divertor target plate. The samples featured a misaligned leading edge and a sloped ridge, respectively. Transient melting by ELMs was induced by moving the outer strike point to the sample location. The different melt patterns observed after exposures at the two sample geometries support the thermionic electron emission model used in the Melt Motion at Surfaces melt motion code, which assumes a strong decrease of the thermionic net current at shallow magnetic field to surface angles. The melt layer transport to less exposed surface areas leads to a ratcheting pile up of re-solidified debris with zonal growth extending from the already enlarged grains at the surface [14].

Experimental simulations of high-energy fluxes of transients expected in fusion reactors are carried in present-day tokamaks such as ASDEX Upgrade or JET. Furthermore, dedicated simulation experiments are performed by using powerful pulsed plasma guns [15], quasi-stationary plasma accelerators (QSPAs) [7, 16–23], linear devices [3, 9, 10] and e-beam facilities [3]. These devices are capable of simulating, at least in part, the loading conditions of interest. The application of such facilities allows to directly obtain data on the erosion of different materials during the plasma-surface interaction under high energy and particle fluxes. For example, melt motion effects driven by external forces have been investigated in previous studies with QSPA Kh-50 and QSPA-T in experiments simulating the expected transient events in ITER [7, 16–18]. It should be mentioned that the plasma pressure in QSPA plasma streams is large compared to those expected for ITER disruptions and ELMs. Nevertheless, increasing the pressure of the impacting plasma stream allows to clarify the contribution of the plasma pressure gradient to the melt motion, even for a QSPA Kh-50 plasma pulse of 0.25 ms duration, and to reach the melt velocities as those expected for ITER disruptions [16]. Whereas in ELM simulation conditions, the influence of the melt motion on the surface profile becomes evident only with a large number of pulses [7, 17–21]. Experimental results on the erosion of castellated targets exposed to a large number of transient plasma loads are most important for the numerical simulation of surface damage effects that are caused by the material melting [4–8, 21] and dust production [9, 10, 19, 20]. It should be noted that the loading conditions relevant to controlled ELMs in ITER (energy density $\sim 0.5\,\mathrm{MJ\,m^{-2}}$, duration 0.25–0.6 ms) are not leading to large melting and melt motion of the affected inclined divertor surfaces [1]. Nevertheless, melt motion becomes the dominant erosion mechanism for uncontrolled ELMs in ITER (energy density up to $4\,\mathrm{MJ\,m^{-2}}$). Therefore, an experimental investigation of the erosion processes on inclined/misaligned castellated tungsten surfaces has been performed within the powerful QSPA Kh-50 with conditions simulating a failure of the ELM control in fusion reactors.

2. Experimental device, sample and diagnostics

The target has been manufactured from sintered tungsten produced by the Plansee AG with a size of $5 \times 5 \times 1\,\mathrm{cm}^3$ with castellation slits. The size of each target unit is $24 \times 12 \times 5\,\mathrm{mm}^3$, which is comparable to monoblocks in ITER. The width of the gaps between the elements is 1 mm. The surface of the target was preliminary exposed to 200 plasma pulses (figure 1(a)) at normal incidence within the QSPA Kh-50 [21]. Since the targets in the ITER divertor will be placed inclined to the plasma flow, the additional plasma exposition of 300 QSPA Kh-50 plasma pulses was applied at an oblique plasma incidence in this experiment. The angle between the direction of the plasma flow and the surface of

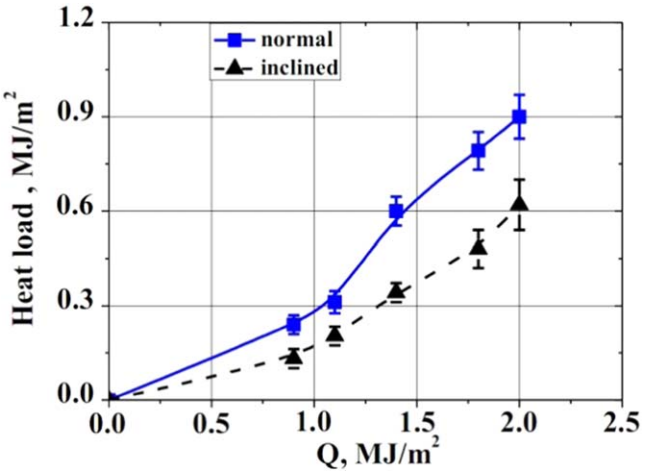

Figure 2. Heat load to the central part of the target surface versus energy density (Q) in the plasma stream for perpendicular and inclined targets.

the target was 30° (figure 1(b)). The target temperature before and between plasma pulses was room temperature. The total number of plasma pulses reached was 500, i.e. about half of the expected number of ELMs during one ITER pulse.

The main parameters of the hydrogen plasma streams were an ion impact energy of about 0.4 keV, a maximum plasma pressure of 0.32 MPa (larger than the plasma pressure relevant to ITER of up to 0.01 MPa), and a stream diameter of 18 cm. It should be noted that the driving force for melt motion was quite small $F = \nabla P_{\mathrm{QSPA}} < 0.2\ \mathrm{MN\,m^{-3}}$ ($D \approx 5$ cm near axis). The temporal plasma pulse shape was approximately triangular with a pulse duration of 0.25 ms, i.e. the plasma load characteristics are close to the plasma load originating from ELMs in ITER [21].

The observation of the plasma interaction with exposed surfaces, the dust particle dynamics, and the droplets monitoring were performed with a high-speed (10 bit CMOS pco.1200 s) digital camera by the PCO AG at exposure times ranging from 1 μs to 1 s and a spatial resolution of 12 × 12 μm^2 within the spectral range from 290 to 1100 nm. In recent experiments, analogous to [19, 21–23], the time of exposition was set to 1.2 ms, allowing a clear registration of particles flying away from the exposed surfaces. Optical diagnostic methods were used for the determination of the main plasma parameters (electron density and temperature) and studies of the impurity behavior during the time of discharge. The surface analysis was carried out with an optical microscope MMR-4 equipped with a CCD camera.

The main feature of the high-power QSPA Kh-50 plasma interaction with targets is the possibility of a dense plasma shield formation close to the target surface [24]. Calorimetric measurements demonstrated that even for plasma exposures that did not result in tungsten melting, the absorbed heat load was about 50% of the impact plasma heat load (figure 2). The plasma layer at the target, formed at the head of the plasma stream, ceased to be completely transparent for subsequently impacting plasma ions [22–24]. This layer of cold plasma was responsible for a decrease in the incident plasma energy that is delivered to the surface. The surface energy load was 0.9 MJ m^{-2} at normal surface incidence (relevant to unmitigated ITER Type I ELMs), i.e. above the melting (0.6 MJ m^{-2}) and below the evaporation (1.1 MJ m^{-2}) thresholds of tungsten (figure 2).

In recent studies with exposures of inclined targets, a decrease of the energy density delivered to the target surface has been observed with a decrease in the incidence angle (figure 2).

The shielding layer is qualitatively visible in figure 1(b), where the bright area corresponds to the region of maximum plasma density. It was found that the thickness of the shielding layer was not uniform over the target surface. The thickness of the shielding layer was smallest at the upstream edge of the sample [22, 23]. As a result, a non-homogeneous distribution of the energy density along the target surface was observed under the inclined incidence. As follows from figure 2, the energy density delivered to surfaces decreases from 0.9 till 0.6 MJ m^{-2} in the center of the target with a decreasing of the angle from 90° till 30°. Nevertheless, the energy density delivered to the leading edge was about 0.9 MJ m^{-2}. It should be noted that the energy density of the incoming plasma was the same for normal and oblique irradiation. Thus, the heat load on the downstream as well as the central parts of the exposed surfaces was smaller than the heat load on the upstream edge. This demonstrated an increasing of the shielding effect for these parts of the target.

3. Erosion of castellated tungsten surfaces exposed to a large number plasma pulses

3.1. Castellated target exposure to 200 plasma pulses at normal incidence

The results of experiments performed earlier [21] on tungsten exposed to 200 plasma pulses at normal incidence showed pronounced melting. Repetitive plasma loads above the melting threshold led to the formation of melted and re-solidified surface layers. Networks of both macro and intergranular cracks appeared on the exposed surfaces. Accumulations of displaced material at the edges of the castellated units were the primary source of splashed droplets due to the development of instabilities in the melted layer. The solid dust ejection was dominated by cracking processes after the end of the pulse and surface re-solidification. Due to the continuously growing crack width (up to ten μm) with the increasing number of pulses, the initially uniform melt pool on the castellated units became disintegrated into a set of melt structures separated by cracks. After a large number of pulses, the progressive corrugation of the surface occurred due to the capillary effects and/or surface tension on exposed W surfaces. It should be noted that the mountains of displaced material at the edges of castellated units developed symmetrically on all outward edges of the target due to the uniform plasma irradiation. In contrast, a non-uniform plasma impact was observed at the oblique QSPA Kh-50 plasma irradiation (figures 1 and 2). Therefore, we performed an irradiation of a

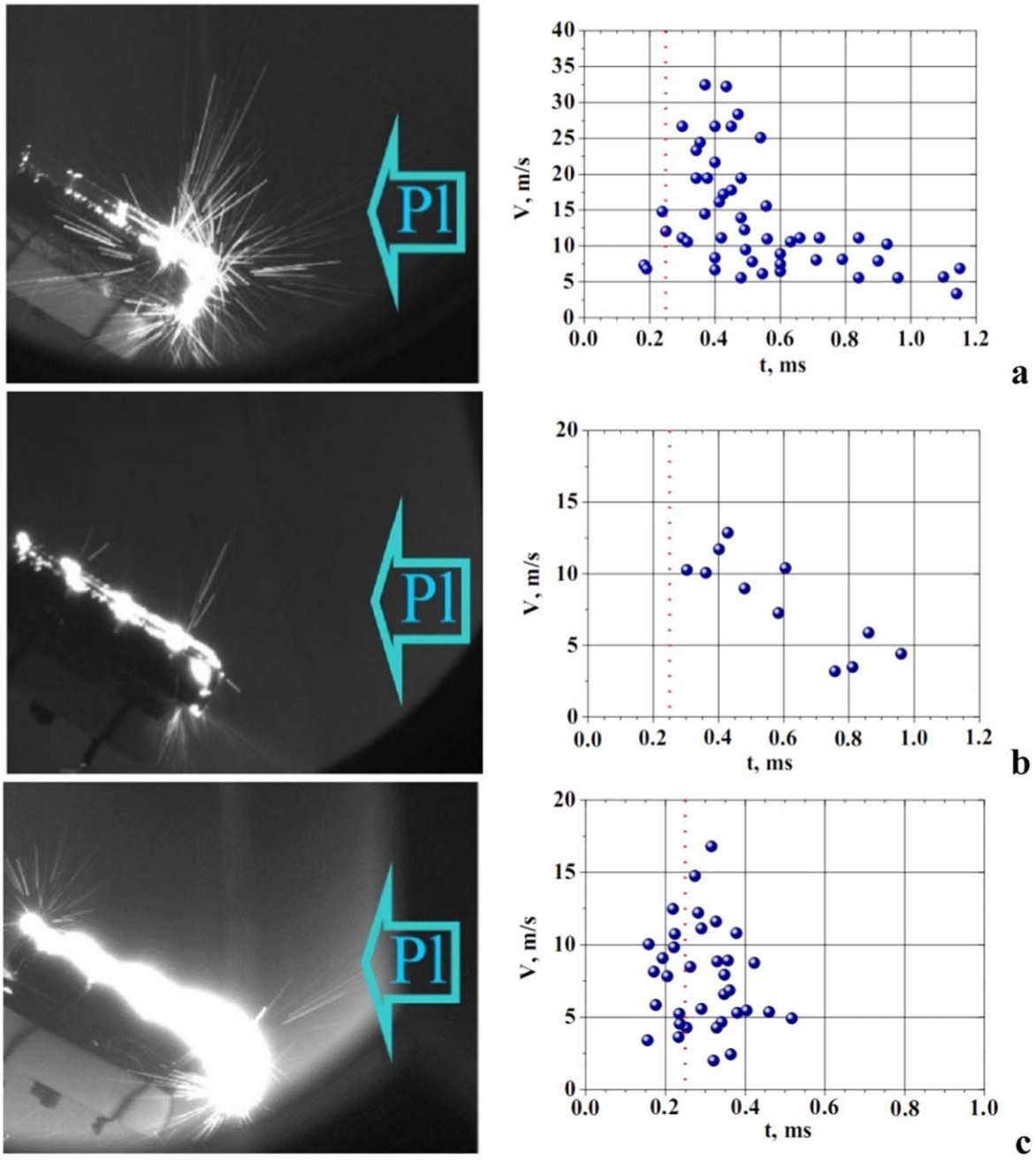

Figure 3. Images of particle traces corresponding to 1.2–2.4 ms after the start of plasma–surface interaction (t_{exp} = 1.2 ms) (left), and the velocity distribution of ejected particles versus particle start-up time from the surface (right) after 20 (a), 80 (b), and 295 (c) plasma pulses. The vertical dotted line indicates the end of the plasma pulse.

pre-damaged target placed oblique to the plasma stream for the evaluation of the erosion of inclined/misaligned castellated tungsten surfaces.

3.2. Castellated target exposure with 300 additional plasma pulses at an oblique plasma incidence

In recent experiments, we applied 300 additional pulses on the castellated tungsten target with a target analysis after 100, 200, and 300 pulses, resulting in a total of 500 plasma pulses. After the initial 20 plasma pulses, the leading edge of the target, which was irradiated by the plasma first, as well as nearby units were locally overheating and intensive ejection of particles occurred (figure 3(a)).

Such particles were mainly flying towards the plasma impact, i.e. in upstream direction. The velocity of the registered particles reached 35 m s^{-1}. Particles with the highest velocities took off at time instances in the range of 0.2–0.4 ms from the beginning of the plasma-surface interaction. Most of the registered particles were ejected from the surfaces after the plasma pulse. With a further increase in the number of plasma pulses, the effect of overheating of exposed surfaces was also observed for other units of the target and the ejection of particles occurred from those parts of the target (figures 3(b)

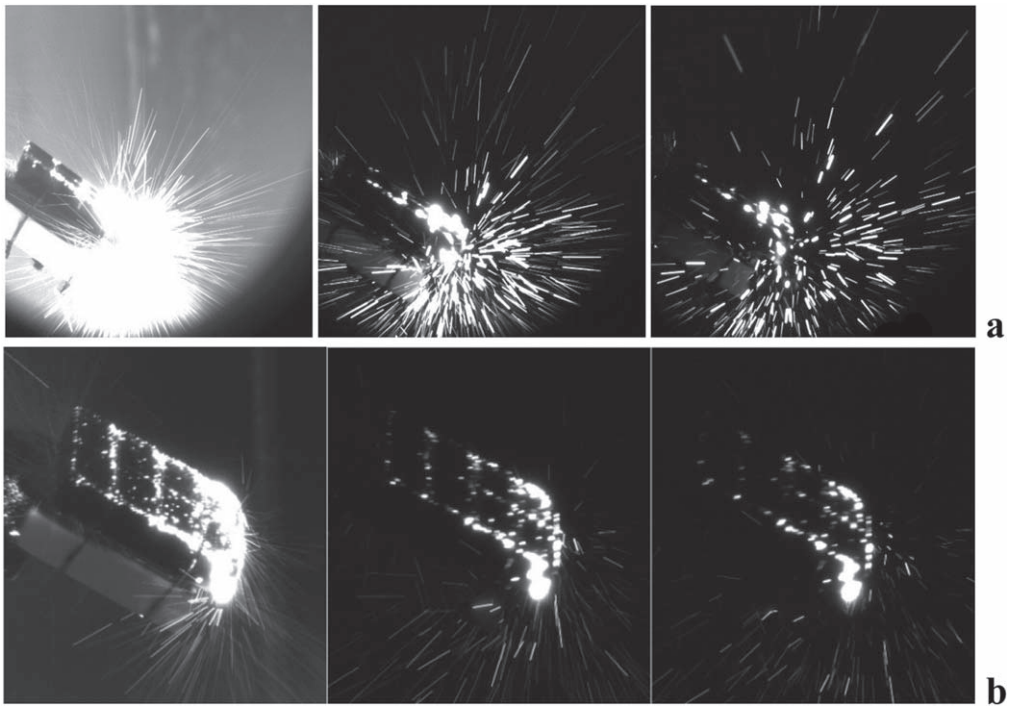

Figure 4. The particle ejection during PSI. Images of droplet traces after 10 (a) and 300 (b) plasma pulses corresponding to 1.2–2.4 ms (left), 3.6–4.8 ms (middle), 6–7.2 ms (right) after the start of the plasma–surface interaction ($t_{\text{exposure}} = 1.2$ ms).

and (c)). The maximum velocity of ejected particles dropped to about 50% of the initial value after 20 plasma pulses, i.e. to less than 18 m s^{-1}. After 200 plasma pulses, the number of ejected particles during the plasma pulse increased (figure 3(c)).

The thickness of the bright area near the exposed surface increased with the plasma pulse number. This could be explained by the influence of cracks and the re-solidified layer on the degradation of the thermal conductivity in a thin near-surface layer after a large numbers of exposures. It should be noted that the observation line was normal to the lateral surface of the tungsten plate during the irradiation with the first 295 plasma pulses (figure 4(a)). Nevertheless, the observation line was adjusted at an additional angle to the surface of the exposed target during the last 5 pulses. Thus, we could observe the overheated parts of the exposed surfaces (figure 4(b)). The overheated leading edge as well as the edges of the target units remained the primary source of ejected particles. Ejected particles continued to be registered after the plasma impact up to >7 ms.

The maximum number of ejected particles was registered during the first 20 plasma pulses (figure 5). The total number of ejected particles decreased significantly to about 10% of the peak value after the first hundred plasma pulses. A saturation of particles ejected from the surfaces except for the leading edge was observed after 100 plasma pulses. An increasing amount of particles ejected from the leading edge was observed after 200 plasma pulses.

For an oblique plasma incidence, the non-uniform plasma layer that formed at the head of the plasma stream was

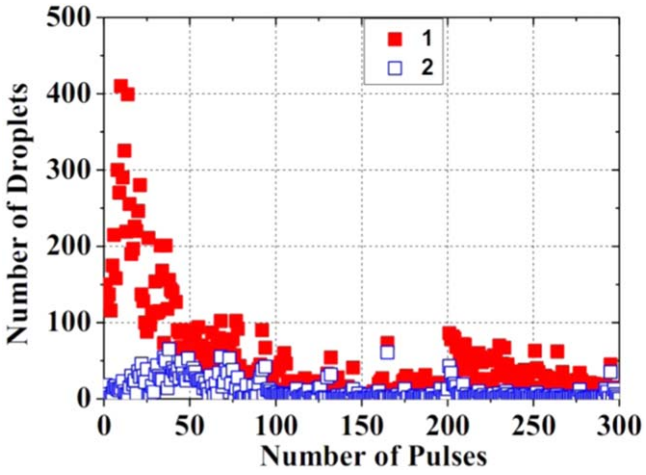

Figure 5. Number of ejected particles versus number of plasma pulses. Filled markers (1) indicate total number of ejected particles, non-filled markers (2) represent the amount of particles ejected from surfaces except for the leading edge.

responsible for a decrease in the incident plasma energy delivered to the target surface [22, 23]. As a result, the induced damage varied over different parts of the target. The erosion of flat surfaces at the downstream part of the target was minimal (figure 6).

The surface of the downstream part of the target remained rather stable with the increasing number of exposures up to 300 pulses. The major crack network with a cell size of up to 1 mm hardly changed. The sequential pulses also smoothed the edges of large cracks, thereby restricting their

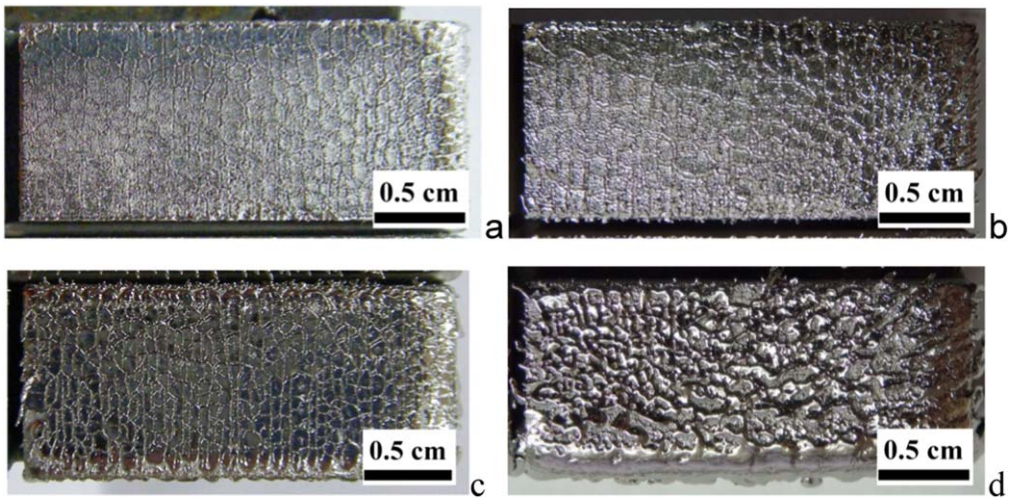

Figure 6. Images of units on downstream (top line) and upstream parts (bottom line) of initial target surfaces (after pre-damaging by 200 normal pulses) (a), (c) and after 300 pulses an oblique (b), (d) plasma incidence.

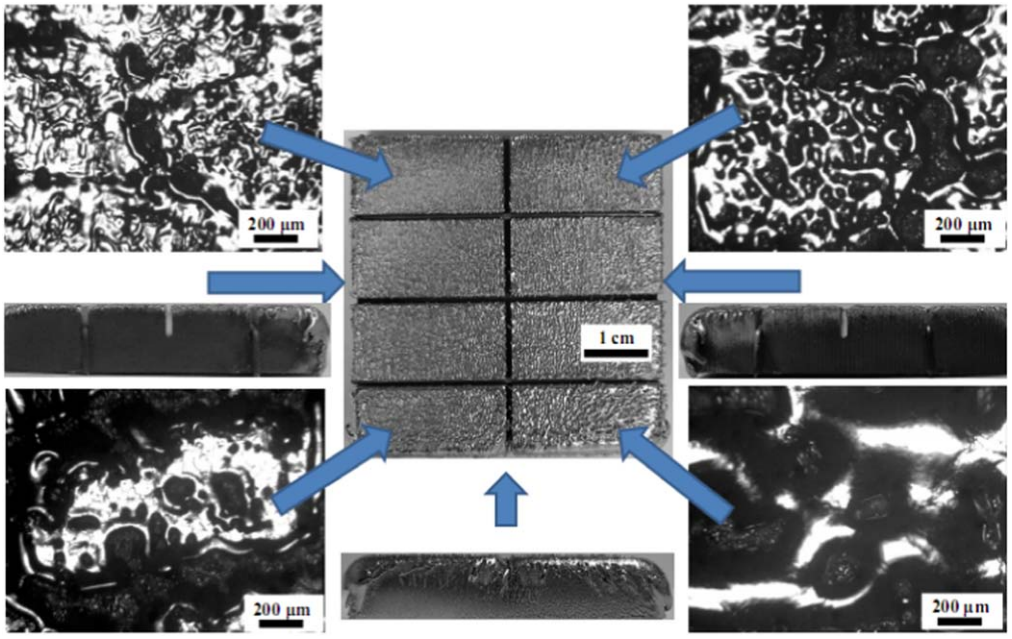

Figure 7. General view and optical microscopy images of different units of the castellated target. The surfaces were exposed to 500 plasma pulses.

growth. It was observed that some molten edges moved into the crack voids. The melt motion covered micro cracks but new ones appeared in places of vanished fractures.

The maximum surface erosion was registered near the leading edge. The large number of repetitive plasma loads above the melting threshold led to the formation of a corrugated re-solidified surface layer on the exposed target due to the capillary/surface tension effects (figure 7).

The motion of the melted material caused the formation of agglomerations of displaced material at the edges of the castellated units. These agglomerations of displaced material (mainly near the leading edge) were the primary sources of the ejected particles. Bridges between the units were not observed with one exception. The melted material filled the gap between the units on the leading edge (figure 8).

4. Discussion and conclusions

For the plasma pulses with a heat load exceeding the melting threshold, melted and re-solidified layers formed on the exposed surfaces. The ejected particles from the molten surfaces originated from Kelvin–Helmholtz (K–H) or Rayleigh–Taylor (R–T) instabilities during the plasma impact as well as surface cracking during surface cooling after the plasma pulse [4–7, 19–23, 25, 26]. The generation of tungsten particles in

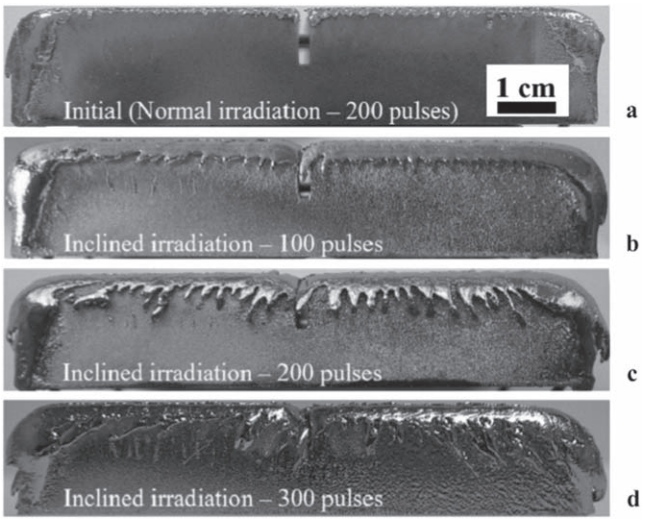

Figure 8. Images of the leading edge after different plasma pulses at 200 normal (a), 100 (b), 200 (c) and 300 (d) addition inclined irradiation.

the form of droplets may occur only during the plasma pulse and (as latest) a few tens of microseconds after the pulse end.

According to the model of the K–H instability growth described in [6], the maximum instability increment γ_{K-H} and wavelength corresponding to it λ_{K-H} are:

$$\gamma_{K-H} = \frac{2p^{\frac{3}{2}}}{3\sigma\sqrt{3\rho_m}}; \quad \lambda_{K-H} = \frac{3\pi\sigma}{p} \tag{1}$$

with the pressure of the plasma (p), the density of the molten material (ρ_m) and the surface tension (σ). For tungsten ($\sigma = 2.48\ \mathrm{H\,m^{-1}}$, $\rho_m = 16.3 \times 10^3\ \mathrm{kg\,m^{-3}}$ [27]) at $p = 0.3$ MPa, the respective values were $\gamma_{K-H} \sim 80\ \mu$m and $1/\gamma_{K-H} \sim 5\ \mu$s. The estimated value of λ_{K-H} is in agreement with the experimentally observed wave like structure on the exposed surfaces (figure 6).

It should be noted that the time (t_{sm}) of the molten layer creation depended on the power density of the plasma stream (P) and the material properties, i.e. the thermal conductivity (k), the specific heat (C_p), the material density (ρ), and the melting temperature (T_m). This time could be estimated from the known formula $t_{sm} = \frac{4}{\pi} k C_p \left(\frac{T_m^2}{P}\right)$. A corresponding estimation of the tungsten melting time resulted in the value of 90–100 μs, which was in a reasonable agreement with the experimental observations and the simulation with the PEGASUS code [15]. Thus, the time of intense melt motion (τ_m) could be estimated as difference between plasma duration of 0.25 ms and t_{sm}.

The R–T instability increment γ_{R-T} corresponds to the wave with the wavelength λ_{R-T} as follows:

$$\gamma_{R-T} = \frac{0.62 V_m^{3/2} \rho_m^{1/4}}{R_{RT}^{3/4} \sigma^{1/4}}; \quad \lambda_{R-T} = \frac{2\pi\sqrt{3\sigma R_{RT}}}{\sqrt{\rho_m V_m^2}}. \tag{2}$$

Here, V_m is the velocity of the melt motion and R_{RT} is the radius of the edge convex. The motion of the liquid film with a thickness of h along the castellated unit edge is stable if the centrifugal force is smaller than the capillary force. The balance of these forces gives the velocity: $V_m = \sqrt{\frac{2\sigma}{\rho_m h}}$. The liquid film separation from the convex corner and further splashing of the melt layer (with depth of h) occur as soon as velocity of the melt motion exceeds V_m [6, 7].

The R–T instability led to the formation of bridges between neighboring castellated units. In this context, the growth of R_{RT} prevented a fast formation of bridges. During the time of intense melt motion (τ_m), the critical edge convex radius is given by

$$R_{RT} \geqslant \frac{0.53\ V_m^2 \rho_m^{1/3} \tau_m^{4/3}}{\sigma^{1/3}}. \tag{3}$$

If R_{RT} is larger than the critical edge convex radius, the growth of the instability and the bridging between the units do not occur [6, 7, 21]. Thus, the surface tension stabilized the growth of the R–T instability. For tungsten at $V_m \sim 5\ \mathrm{m\,s^{-1}}$, the calculated values are $R_{RT} \sim 3$ mm, $1/\gamma_{R-T} \sim 48\ \mu$s, and $\lambda_{R-T} \sim 0.8$ mm.

The estimated values of $1/\gamma_{K-H}$ and $1/\gamma_{R-T}$ are less than the duration of the plasma irradiation. Thus, K–H and R–T instabilities could develop during the plasma surface interaction. Nevertheless, the K–H instability develops faster than the R–T instability due to $1/\gamma_{K-H}$ being less than $1/\gamma_{R-T}$.

The velocity U of the droplet ejection can be estimated with the assumption of the equality of the kinetic energy $E_k = \frac{1}{2}\rho_m U^2 \frac{4}{3}\pi r_d^3$ of the given droplet with the radius (r_d) and the surface energy of the same droplet $E_s = 4\pi\sigma\ r_d^2$ as:

$$U \geqslant \sqrt{\frac{24\sigma}{\lambda\rho_m}}, \tag{4}$$

where $\lambda = 4r_d$ is the wavelength of the K–H or R–T instabilities [6, 7].

For the K–H instability, the velocity of the ejected droplets was $U \sim 7\ \mathrm{m\,s^{-1}}$. For the R–T instability, the velocity of the particles was $U \sim 3\ \mathrm{m\,s^{-1}}$. After a small number of plasma pulses, the average speed of particles ejected during the plasma impact was near $10\ \mathrm{m\,s^{-1}}$ (figure 3). Hence, such particles were ejected due to the development of a K–H instability. After many plasma pulses, the speed of the ejected particles decreased. This implied that particles were ejected due to the development of K–H as well as R–T instabilities. Estimations of the wavelength and increment for both instabilities agreed with the observed surface relief and the duration of the plasma pulses. A significant growth of R_{RT} was registered on the leading edge after a large number of plasma pulses (figure 8).

Other ejected particles may be exclusively solid dust that was generated due to elastic energy stored in the stressed re-solidified tungsten surface layer. The solid dust ejection was dominated by cracking processes after the end of pulse in the course of the surface re-solidification. The velocity (U_{ts}) of such particles is determined by the difference of the thermal stress energy and the cohesive binding energy [9, 10, 25, 26]

as follows:

$$U_{ts} = \Delta\alpha T\left[\frac{2E}{\rho(1-\mu)}\right]^{1/2}\left[1-\frac{r_{min}}{r}\right]^{1/2};$$
$$r_{min} = \frac{\sigma_s(1-\mu)}{(\Delta\alpha T)^2 E}. \quad (5)$$

Here, α is the thermal expansion coefficient, T is the absolute temperature, E is the modulus of elasticity, μ is the Poisson's ratio, and $\Delta(\alpha T)$ is the difference of αT values between the grain and substrate. r_{min} is the minimum size of a particle at which the particle is detached from the substrate. $\sigma_s = 4.3\ \mathrm{J\,m^{-2}}$ is the free surface energy [10].

The estimation showed that the maximum velocity ($U_{ts} \sim 40\ \mathrm{m\,s^{-1}}$) of dust particles was larger than the velocity of droplets ejected due to the development of instabilities in the molten layer. It should be noted that the velocity of dust particles decreased with the reduction of the surface temperature. This behavior is in agreement with the measured decreasing particle speed at later times (figure 3).

The melt layer tended to be transformed into a corrugated structure on exposed surfaces (figures 6 and 7). This evolution coincided with the surface cracking. With increasing the pulse number, the crack width gradually increased up to 20 μm. The melt pool on the castellated units disintegrated into a set of melt structures separated by cracks. A further increase of the plasma pulse number (above 200) led to considerable qualitative changes of the surface morphology. Each cell of the crack network was strongly subjected to the surface tension that minimized the melt pool area. After several hundreds of exposures, the progressive corrugation of the surface occurred due to the capillary/surface tension effects on the exposed W surfaces. At this point, the damage caused by cracking became dominant. It should be noted that tungsten cracking cannot be completely mitigated by the preheating above the ductile-brittle transition temperature [17]. For the preheated target with the surface loads capable of melting, the surface cracking was accompanied by swelling, which demonstrated the influence of the surface tension resulting from the formation of 'micro-brush' structures similar to the W-targets exposed at the room temperature.

The erosion of an inclined castellated tungsten target under ITER relevant transient heat loads has been studied using the powerful QSPA Kh-50. It was found that the loading conditions led to pronounced melting of the affected surfaces. Intense overheating of the leading edge, which interacted with plasma first, was observed accompanied by the formation of an excrescence of shifted material during first few tens of plasma pulses. This re-solidified material agglomeration was the predominant source of ejected particles. The maximum number of ejected particles was registered after the plasma pulses, i.e. during the cooling process. Nevertheless, the amount of particles ejected during the plasma exposure increased with the plasma pulse number (figure 3). A large number (above 200) of repetitive plasma loads led to the formation of a corrugated wave-like re-solidified surface layer due to the capillary/surface tension effects on the exposed tungsten surfaces. A suppression of droplets splashing and dust ejection from the flat surfaces of castellated monoblocks was registered, whereas the edges remained sources of ejected particles. The leading edge was the primary source of ejected particles.

The inclination of targets lead to an increase the plasma projection angle to the surface and thus to the distribution of the impacting energy over a larger area (decrease of the specific load). As a result, major damages were recognized near leading edge. Castellated surfaces can be transformed to a flat profile due to the formation of bridges between the units (including the leading edge). The influence of cracks and the surface tension force on the degradation of the thermo-physical properties of a thin near-surface layer after a large numbers of exposures can be important for the fusion reactor operation. Any leading edges of castellated targets are the primary sources of liquid/dust particles in case of pronounced surface melting. Therefore, more detailed experimental and theoretical studies of the surface damaging mechanisms of castellated tungsten targets above and below the melting thresholds, as well as the influence of preheating on the erosion processes, are required.

Acknowledgments

'This work has been carried out within the framework of the EUROfusion Consortium and has received funding from the Euratom research and training programme 2014–2018 and 2019–2020 under grant agreement No. 633053. The views and opinions expressed herein do not necessarily reflect those of the European Commission.' Work performed under EUROfusion WP PFC. This work has also been supported by National Academy Science of Ukraine project X-2-11-10/2019, П-5/24-2019 and IAEA's CRP F43022.

ORCID iDs

V A Makhlai https://orcid.org/0000-0002-5258-7793
S S Herashchenko https://orcid.org/0000-0003-1449-4884
I E Garkusha https://orcid.org/0000-0001-6538-6862
M Wirtz https://orcid.org/0000-0002-1857-688X
B Spilker https://orcid.org/0000-0001-9921-0291

References

[1] Pitts R A *et al* 2017 *Nucl. Mater. Energy* **12** 60–74
[2] Hirai T *et al* 2016 *Nucl. Mater. Energy* **9** 616–22
[3] Brezinsek S *et al* 2017 *Nucl. Fusion* **57** 116041
[4] Miloshevsky G and Hassanein A 2011 *J. Nucl. Mater.* **415** S74
[5] Miloshevsky G and Hassanein A 2013 *J. Nucl. Mater.* **438** S155
[6] Bazylev B N and Landman I S 2007 *Problems Atomic Sci. Technol.* **1** 35–9
[7] Bazylev B *et al* 2007 *J. Nucl. Mater.* **363–365** 1011
[8] Igitkhanov Y *et al* 2015 *Fusion Sci. Technol.* **68** 516

[9] De Angel M *et al* 2017 Remobilization of tungsten dust from castellated plasma-facing components *Nucl. Mater. Energy* **12** 536–40
[10] Ratynskaia S *et al* 2017 Tungsten dust remobilization under steady-state and transient plasma Conditions *Nucl. Mater. Energy* **12** 569–74
[11] Thoren E *et al* 2017 *Phys. Scr.* **T170** 014006
[12] Thoren E *et al* 2018 *Nucl. Fusion* **58** 106003
[13] Krieger K *et al* 2018 *Nucl. Fusion* **58** 026024
[14] Thorén E *et al* 2018 *Nucl. Mater. Energy* **17** 194–9
[15] Pestchanyi S *et al* 2017 *Fusion Eng. Design* **24** 401–4
[16] Tereshin V I *et al* 2003 *J. Nucl. Mater.* **313–316** 685
[17] Garkusha I E *et al* 2009 *J. Nucl. Mater.* **386–388** 127–31
[18] Garkusha I E *et al* 2007 *J. Nucl. Mater.* **363–365** 1021
[19] Garkusha I E *et al* 2014 *Fusion Sci. Technol.* **65** 186–93
[20] Pestchanyi S *et al* 2014 *Fusion Sci. Technol.* **66** 150
[21] Makhlai V A *et al* 2019 *Nucl. Mater. Energy* **19** 493–7
[22] Chuvilo A A *et al* 2012 *Nukleonika* **57** 49–53
[23] Herashchenko S S *et al* 2014 *Problems Atomic Sci. Technol.* **6** 44–7
[24] Tereshin V I *et al* 2007 *Plasma Phys. Control. Fusion* **49** A231–9
[25] Martynenko Y V and Yu N M 2012 *Plasma Phys. Rep.* **38** 290–4
[26] Martynenko Y V 2017 *Plasma Phys. Rep.* **43** 324–9
[27] Tolias P *et al* 2017 *Nucl. Mater. Energy* **13** 42–57